Table 1 Predicted values of scaling exponents for physiological and anatomical variables of plant vascular systems.

Variable	Plant mass		Branch radius		
	Exponent predicted	Symbol	Symbol	Exponent	
				Predicted	Observed
Number of leaves	$\frac{3}{4}$ (0.75)	n_0^L	n_k^L	2 (2.00)	2.007 (ref. 12)
Number of branches	$\frac{3}{4}$ (0.75)	N_0	N_k	–2 (–2.00)	–2.00 (ref. 6)
Number of tubes	$\frac{3}{4}$ (0.75)	n_0	n_k	2 (2.00)	n.d.
Branch length	$\frac{1}{4}$ (0.25)	l_0	l_k	$\frac{2}{3}$ (0.67)	0.652 (ref. 6)
Branch radius	$\frac{3}{8}$ (0.375)	r_0			
Area of conductive tissue	$\frac{7}{8}$ (0.875)	A_0^{CT}	A_k^{CT}	$\frac{7}{3}$ (2.33)	2.13 (ref. 8)
Tube radius	$\frac{1}{16}$ (0.0625)	a_0	a_k	$\frac{1}{6}$ (0.167)	n.d.
Conductivity	1 (1.00)	K_0	K_k	$\frac{8}{3}$ (2.67)	2.63 (ref. 12)
Leaf-specific conductivity	$\frac{1}{4}$ (0.25)	L_0	L_k	$\frac{2}{3}$ (0.67)	0.727 (ref. 17)
Fluid flow rate			$\dot{Q}_k$	2 (2.00)	n.d.
Metabolic rate	$\frac{3}{4}$ (0.75)	$\dot{Q}_0$			
Pressure gradient	$-\frac{1}{4}$ (–0.25)	$\Delta P_0/l_0$	$\Delta P_k/l_k$	$-\frac{2}{3}$ (–0.67)	n.d.
Fluid velocity	$-\frac{1}{8}$ (–0.125)	u_0	u_k	$-\frac{1}{3}$ (–0.33)	n.d.
Branch resistance	$-\frac{3}{4}$ (–0.75)	Z_0	Z_k	$-\frac{1}{3}$ (–0.33)	n.d.
Tree height	$\frac{1}{4}$ (0.25)	h			
Reproductive biomass	$\frac{3}{4}$ (0.75)				
Total fluid volume	$\frac{25}{24}$ (1.0415)				

Values are given as a function of total plant mass, M, and branch radius, r_k. For the latter case, predictions are compared with measured values in the last column. References cited do not quote confidence levels, except for branch length, where they are given as ±0.036. Because botanists rarely report allometric scaling with mass, no values for observed exponents are quoted. n.d., no data available.

ferns, grasses and saplings with few branches, so that $\gamma \rightarrow n^{-1/2}$ rather than $n^{-1/3}$, leading to $l_k \propto r_k$ (refs 7, 15); and (6) constrictions in tubes at petioles and perhaps at other branch junctions[4,16]. These complications are expected to have small effects, because many quantities, such as scaling exponents, effectively average out over the whole plant.

The model quantitatively predicts how vessels must taper to compensate for variation in total transport path length. This is supported by measured changes in vessel radius and resistance within and between plants[4,11] and leads to a maximum height for trees. An important consequence is that tapering ensures comparable xylem flow to all leaves. Competition for light has apparently led to a design that maximizes canopy height and simultaneously minimizes tapering of vascular tubes. In a given environment with a fixed pressure differential between air and soil, on average all xylem tubes of all plants conduct water and nutrients at approximately the same rate. This counterintuitive result provides the fundamental basis for the recently demonstrated equivalence of resource use, independent of plant size, across diverse ecosystems[21].

The model shows that quarter-power allometric scaling laws, which are well known in animals[1], also apply to many characteristics of plants[2]. There are many parallels: in both, metabolic rate scales as $M^{3/4}$, radius of trunk and aorta as $M^{3/8}$, and size of and fluid velocity in terminal vessels as M^0. It seems that these scaling laws are nearly universal in biology, and that they have their origins in common geometric and hydrodynamic principles that govern the transport of essential materials to support cellular metabolism. □

Received 27 November 1998; accepted 20 May 1999.

1. Schmidt-Nielsen, K. *Scaling: Why is Animal Size so Important?* (Cambridge Univ. Press, Cambridge, 1984).
2. Niklas, K. J. *Plant Allometry: The Scaling of Form and Process* (Univ. of Chicago Press, Chicago, 1994).
3. West, G. B., Brown, J. H. & Enquist, B. J. A general model for the origin of allometric scaling laws in biology. *Science* **276,** 122–126 (1997).
4. Zimmermann, M. H. *Xylem Structure and the Ascent of Sap* (Springer, New York, 1983).
5. Tyree, M. T. & Ewers, F. W. The hydraulic architecture of trees and other woody plants. *New Phytol.* **119,** 345–360 (1991).
6. Shinozaki, K., Yoda, K., Hozumi, K. & Kira, T. A quantitative analysis of plant form—the pipe model theory: I. Basic analysis. *Jpn. J. Ecol.* **14,** 97–105 (1964).
7. Bertram, J. E. A. Size-dependent differential scaling in branches: the mechanical design of trees revisited. *Trees* **4,** 241–253 (1989).
8. Patino, S., Tyree, M. T. & Herre, E. A. Comparison of hydraulic architecture of woody plants of differing phylogeny and growth form with special reference to free standing and hemi-epiphytic *Ficus* species from Panama. *New Phytol.* **129,** 125–134 (1995).
9. Kuuluvainen, T., Sprugel, D. G. & Brooks, J. R. Hydraulic architecture and structure of *Abies lasiocarpa* seedlings in three alpine meadows of different moisture status in the eastern Olympic mountains, Washington, U.S.A. *Arct. Alp. Res.* **28,** 60–64 (1996).
10. Yang, S. & Tyree, M. T. Hydraulic architecture of *Acer saccharum* and *A. rubrum*: comparison of branches to whole trees and the contribution of leaves to hydraulic resistance. *J. Exp. Bot.* **45,** 179–186 (1994).
11. Ewers, F. W. & Zimmermann, M. H. The hydraulic architecture of eastern hemlock *Tsuga canadensis*. *Can. J. Bot.* **62,** 940–946 (1984).
12. Yang, S. & Tyree, M. T. Hydraulic resistance in *Acer saccharum* shoots and its influence on leaf water potential and transpiration. *Tree Physiol.* **12,** 231–242 (1993).
13. Long, J. N., Smith, F. W. & Scott, D. R. M. The role of Douglas fir stem sapwood and heartwood in the mechanical and physiological support of crowns and development of stem form. *Can. J. For. Res.* **11,** 459–464 (1981).
14. Rogers, R. & Hinckley, T. M. Foliar weight and area related to current sapwood area in oak. *Forest Sci.* **25,** 298–303 (1979).
15. Niklas, K. J. Size-dependent allometry of tree height, diameter and trunk taper. *Ann. Bot.* **75,** 217–227 (1995).
16. Tyree, M. T. & Alexander, J. D. Hydraulic conductivity of branch junctions in three temperate tree species. *Trees* **7,** 156–159 (1993).
17. Tyree, M. T., Graham, M. E. D., Cooper, K. E. & Bazos, L. J. The hydraulic architecture of *Thuja occidentalis*. *Can J. Bot.* **61,** 2105–2111 (1983).
18. Fitter, A. H. & Strickland, T. R. Fractal characterization of root system architecture. *Funct. Ecol.* **6,** 632–635 (1992).
19. Morse, D. R., Lawton, J. H., Dodson, J. H. & Williamson, M. M. Fractal dimension of vegetation and the distribution of arthropod body lengths. *Nature* **314,** 731–733 (1985).
20. McMahon, T. A. & Kronauer, R. E. Tree structures: deducing the principle of mechanical design. *J. Theor. Biol.* **59,** 443–436 (1976).
21. Enquist, B. J., Brown, J. H. & West, G. B. Allometric scaling of plant energetics and population density. *Nature* **395,** 163–165 (1998).
22. Turcotte, D. L., Pelletier, J. D. & Newman, W. I. Networks with side branching in biology. *J. Theor. Biol.* **193,** 577–592 (1998).

Acknowledgements. We thank K. Niklas and M. Tyree for comments. J.H.B. was supported by the NSF, B.J.E. by the NSF and with an NSF post-doctoral fellowship, and G.B.W. by the US Department of Energy. We also thank the Thaw Charitable Trust for support.

Correspondence and requests for materials should be addressed to B.J.E. (e-mail: benquist@unm.edu).

Dynamics of disease resistance polymorphism at the *Rpm1* locus of *Arabidopsis*

Eli A. Stahl*, Greg Dwyer†, Rodney Mauricio†, Martin Kreitman*† & Joy Bergelson*†

* *Committee on Genetics,* †*Department of Ecology and Evolution, University of Chicago, Chicago, Illinois 60637, USA*

The co-evolutionary 'arms race'[1] is a widely accepted model for the evolution of host–pathogen interactions. This model predicts that variation for disease resistance will be transient, and that host populations generally will be monomorphic at disease-resistance (*R*-gene) loci. However, plant populations show considerable polymorphism at *R*-gene loci involved in pathogen recognition[2]. Here we have tested the arms-race model in *Arabidopsis thaliana* by analysing sequences flanking *Rpm1*, a gene conferring the ability to recognize *Pseudomonas* pathogens carrying *AvrRpm1* or *AvrB* (ref. 3). We reject the arms-race hypothesis: resistance and susceptibility alleles at this locus have co-existed for millions of years. To account for the age of alleles and the relative levels of polymorphism within allelic classes, we use coalescence theory to model the long-term accumulation of nucleotide polymorphism in the context of the short-term ecological dynamics of disease resistance. This analysis supports a 'trench warfare' hypothesis, in which advances and retreats of resistance-allele frequency maintain variation for disease resistance as a dynamic polymorphism[4,5].

Arabidopsis thaliana exhibits a disease-resistance polymorphism in which susceptible individuals are completely lacking *Rpm1* (refs 3, 6). The presence of *Rpm1* homologues in *Brassica*[6] and the closely

related species *Arabidopsis* (or *Arabis*)[7] *lyrata* indicates that the polymorphism arose through deletion of *Rpm1* in an *Arabidopsis* ancestor. A sample of 26 *A. thaliana* accessions (Table 1), randomly chosen from throughout the species' geographic range, yields an *Rpm1* resistance-allele frequency of 0.52 (s.e. = 0.098). Dip tests[8] challenging plants with transgenic pathogen strains confirm that *Rpm1* presence confers recognition of *AvrRpm1* and disease resistance. Thus, variation at *Rpm1* affects disease-resistance phenotype, with both resistant and susceptible individuals distributed across the range of *A. thaliana*.

We used population genetic theory to formulate testable predictions arising from the arms-race hypothesis. Specifically, continual selective turnover of alleles is a hallmark of this model[9], and theory for selective sweeps[10] predicts that resistance alleles should be young and nearly identical in sequence to susceptibility alleles. In contrast, long-lived variation for resistance is an alternative outcome of ecological models of gene-for-gene interactions[11,12], and theory for balanced polymorphism[13] predicts old resistance and susceptibility alleles that differ substantially in DNA sequence, especially near the site under selection. These alternative hypotheses make opposing predictions about variation among alleles, and they can be distinguished by testing data against a null model of neutral molecular evolution[14].

To carry out this test, we characterized variability among resistance and susceptibility alleles in our accession sample (Table 1) by sequencing 1,710 base pairs (bp) 5′ and 948 bp 3′ of the *Rpm1* deletion 'junction'. Figure 1 shows the genealogy of the junction region, giving relationships among the 27 *A. thaliana* alleles and one allele from the outgroup species *A. lyrata*. This genealogy differs significantly from a neutral genealogy in that too many of the changes fall on the branches separating the two allelic classes relative to those within allelic classes (Tajima's D (ref. 15) = 3.06, $P < 0.001$). Furthermore, sliding-window analysis of allelic and species divergence across the junction region (Fig. 2) shows a dramatic peak of polymorphism that is centred at the site of the *Rpm1* disease-resistance polymorphism and that decays on both sides. The ratio of polymorphism to divergence is significantly heterogenous across the junction region compared to neutral expectations (Runs test[16], $P < 0.005$), owing to the peak of polymorphism associated with *Rpm1*. At the junction, divergence between resistance and susceptibility alleles reaches 11.8%, approximately equal to the 10.5% average divergence between *A. thaliana* and *A. lyrata*, and similar to species divergence for synonymous and noncoding sites at other loci[17–20]. At a substitution rate of 6×10^{-9} per site per year[21], this level of divergence indicates that the *Rpm1* polymorphism arose around 9.8 million years (Myr) ago.

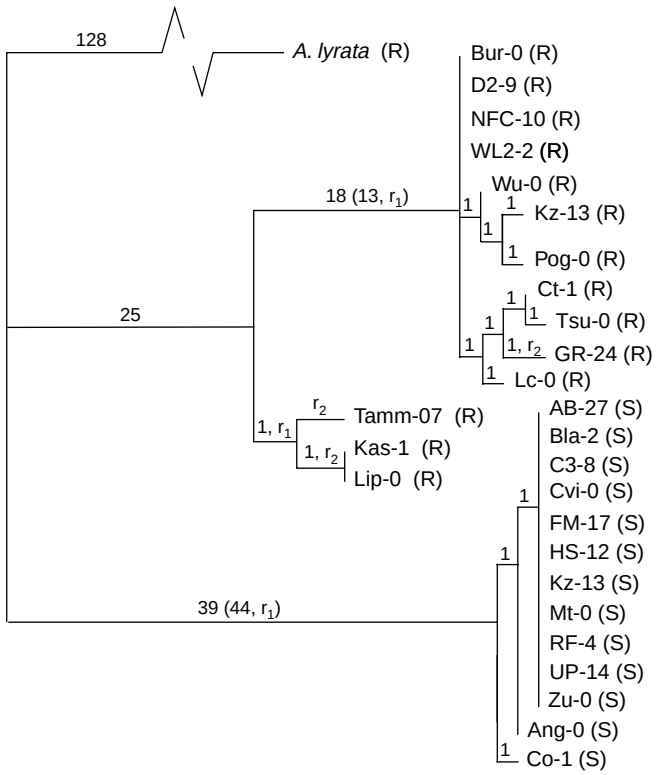

Figure 1 Genealogy of the *Rpm1* junction region. Alleles are named by accession, with *Rpm1* genotypes resistance (R) or susceptibility (S) in parentheses. This tree is one of fifteen most parsimonious trees, which differ in the branching within the R allelic class. The divergence between two clusters of R alleles is attributable to a recombination event (r_1) between R and S alleles at the 5′ end of the sequenced region, involving 18 polymorphic sites (13 and 5 placed on the R and S lineages, respectively). Numbers above branches reflect a placement of nucleotide mutations taking into account two inferred recombination events, r_1 (above) and r_2 within the R allelic class. In assuming that mutations shared by non-recombinant R alleles (Bur-0 cluster) are differences between R and S alleles rather than within the R allelic class, this placement affects only the results of our intraclass polymorphisms analysis and is conservative.

Table 1 Accession sample *Rpm1* genotypes and phenotypes

Accession	Origin	Genotype	Phenotype vs. *AvrRpm1*
Bur-0	Ireland	Rpm1/Rpm1	resistance
Ct-0	Italy	Rpm1/Rpm1	resistance
D2-9*	N. Carolina, USA	Rpm1/Rpm1	resistance
GR-24*	Michigan, USA	Rpm1/Rpm1	resistance
Kas-1	India	Rpm1/Rpm1	resistance
Lc-0	Scotland	Rpm1/Rpm1	resistance
Lip-0	Poland	Rpm1/Rpm1	resistance
NFC-10*	England	Rpm1/Rpm1	n.d.
Pog-0	British Columbia, Canada	Rpm1/Rpm1	resistance
Tamm-07*	Finland	Rpm1/Rpm1	n.d.
Tsu-0	Japan	Rpm1/Rpm1	resistance
WL2-2*	N. Carolina, USA	Rpm1/Rpm1	resistance
Wu-0	Germany	Rpm1/Rpm1	resistance
Kz-13*	Kazakistan	Rpm1/rpm1	resistance
AB-27*	Indiana, USA	rpm1/rpm1	disease
Ang-0	Belgium	rpm1/rpm1	disease
Bla-2	Spain	rpm1/rpm1	disease
C3-8*	N. Carolina, USA	rpm1/rpm1	disease
Co-1	Portugal	rpm1/rpm1	disease
Cvi-0	Cape Verdi Island	rpm1/rpm1	disease
FM-17*	New York, USA	rpm1/rpm1	disease
HS-12*	Massachusetts, USA	rpm1/rpm1	disease
Mt-0	Libya	rpm1/rpm1	disease
RF-4*	Indiana, USA	rpm1/rpm1	n.d.
UP-14*	Michigan, USA	rpm1/rpm1	disease
Zu-0	Switzerland	rpm1/rpm1	disease

Genotypes are presence or absence of *Rpm1* determined by PCR. Both alleles of Kz-13 were included in population genetic analyses on the assumption that heterozygosity resulted from recent outcrossing, so the 26 accession random sample includes 27 alleles. The observed resistance-allele frequency 0.52 is not sensitive to accessions' source, field collected (asterisks) versus stock centre, or geographic origin. Phenotypes after innoculation with *Pseudomonas syringae* DC3000 with *AvrRpm1* (see Methods) are resistance, disease or not determined (n.d.). All lines (except NFC-10, Tamm-07 and RF-4, which were not tested) exhibited disease when challenged with the control strain, DC3000 without *AvrRpm1*.

Having rejected neutrality based on the Tajima's D and Runs tests, we can entertain two alternatives to natural selection maintaining resistance and susceptibility alleles. One possibility is that many nucleotide changes occurred in the same mutational event as the *Rpm1* deletion. If this were true then the point mutations should be associated with the susceptibility allele. However, there are similar numbers of changes on the resistance and susceptibility lineages (Fig. 1, $\chi^2_{1df} = 0.44$). Even if many point mutations occurred on both alleles in the individual suffering the *Rpm1* deletion of one allele, it is highly improbable that this particular undeleted resistance allele would have come to replace all other resistance alleles in the species.

A second alternative is that resistance and susceptibility alleles originated 9.8 Myr ago in a geographically subdivided population and have persisted in separate subpopulations until the recent past. Under this scenario, a signature of haplotypic divergence should be

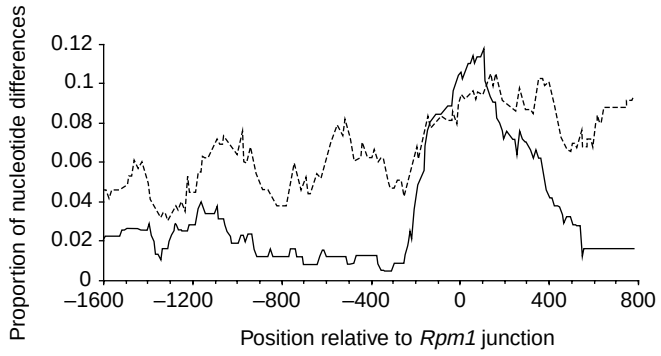

Figure 2 Sliding window analysis. The average pairwise proportion of nucleotide differences are shown between resistance and susceptibility alleles (solid line), and between all *A. thaliana* alleles and the *A. lyrata* sequence (dashed line). Values are midpoints of 250-bp windows (adjusted to exclude gaps). Position is relative to the *Rpm1* deletion (0 bp, not shown), so that negative and positive positions are, respectively, 5′ and 3′ of the *Rpm1* cds.

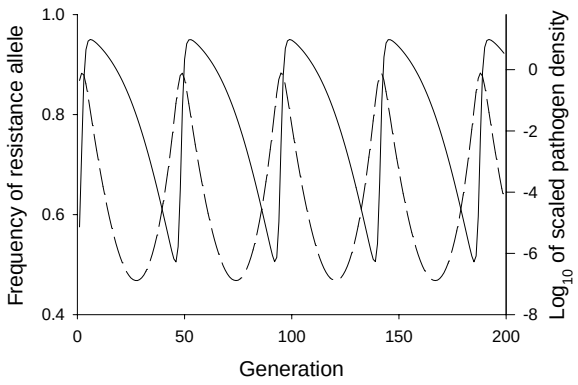

Figure 3 Model for an *A. thaliana–Pseudomonas* interaction. Host resistance allele frequency (solid line) and pathogen density (dashed line) are shown for a model that includes a cost of resistance and yearly frequency-dependent epidemics. The trajectory shown here gives a ratio of polymorphism within resistance and susceptibility allelic classes of 5.71, which compares well with the observed value of 5.72. Long-period cycles in the frequency of resistance are required for the model to achieve a good fit to the polymorphism data.

present across the genome. Our own coalescence simulations of subdivided populations (see Methods) find that the configuration of polymorphism at *Rpm1* is inconsistent with a subdivision explanation. Although the haplotypes corresponding to the two *Rpm1* allelic classes extend across the sequenced region, polymorphic sites are too clustered within the region. Thus, the *Rpm1* sequence data reject the arms-race hypothesis in favour of an alternative that leads to the selective maintenance of variation for disease resistance.

Although the arms-race hypothesis cannot explain the divergence between resistance and susceptibility alleles, a succession of positively selected resistance alleles is still possible. We examined divergence between *A. lyrata* and resistant *A. thaliana* accession Col-0 (ref. 3) across the entire *Rpm1* coding sequence to look for an accelerated amino-acid substitution rate indicative of positive selection[14]. On the contrary, amino-acid replacements have accumulated at a much slower rate than synonymous changes[22] ($K_a = 0.028$ and $K_s = 0.13$). In addition, the 55 amino-acid substitutions between the two species are scattered throughout the coding sequence rather than being associated with the leucine-rich repeat region, the putative pathogen-recognition domain[2,3] ($\chi^2_{1df} = 0.11$). Selectively driven turnover of resistance alleles does not appear to be important in RPM1 protein evolution.

Our data indicate, therefore, that the two alleles at *Rpm1* represent a long-lived polymorphism maintained by natural selection rather than the result of a co-evolutionary arms race. How does selection act to maintain this polymorphism? Because an *Rpm1*-null allele confers susceptibility, ecological trade-offs for allelic resistance specificities cannot apply here. Heterozygote advantage is also ruled out by *A. thaliana*'s extremely low outcrossing rate[23]. Maintenance of this polymorphism therefore requires a balance between selection for disease resistance and a cost of resistance in the absence of the pathogen[24], and further requires temporal or geographic variation in selection.

Indeed, variability within allelic classes at *Rpm1* suggests temporal variation in selection. For a long-lived polymorphism maintained by natural selection at a constant frequency, the number of linked neutral segregating sites within an allelic class is expected to be proportional to its frequency[13]. However, resistance alleles of *Rpm1* segregate for ten times as many polymorphisms as do susceptibility alleles (30 versus 3), despite the fact that both alleles are approximately equally frequent. Excluding intraclass polymorphisms that may have arisen by rare recombination events between allelic classes (Fig. 1), we conservatively estimate that resistance and susceptibility allelic classes have 12 and 3 intraclass polymorphisms, respectively. Under a model of balancing selection at a constant frequency (see Methods), these numbers of intraclass polymorphisms are expected for a resistance-allele frequency of 0.81, a significantly higher value than our worldwide estimate of 0.52. Furthermore, the resistance allelic class contains too many of the intraclass polymorphisms for a parametric *Rpm1* allele frequency of 0.52 ($P = 0.0377$). The data therefore indicate that the frequency of resistance at *Rpm1* may have fluctuated over time.

Temporal variation arises in host–pathogen interactions because disease spread is more likely when the frequency of resistance is low. This frequency-dependent selection can lead to the periodic recurrence of severe epidemics, causing the frequency of resistance to cycle[11,12]. To determine whether frequency-dependent epidemics can account for the *Rpm1* population genetic data, we constructed and analysed a model describing an *A. thaliana–Pseudomonas* interaction. Our model differs from previous models in allowing *Pseudomonas* to survive between epidemics in nonpathogenic populations[25]. Figure 3 shows model results leading to long-lived polymorphism and long-period cycles in the frequency of resistance. The cycles attain the observed resistance-allele frequency and give rise to the observed variability within allelic classes. Our data are consistent with a model in which variation for disease resistance is maintained by frequency-dependent selection, and thus provide, to our knowledge, the first empirical evidence for dynamical polymorphism, a phenomenon that Hamilton and co-workers[5,12] have argued is likely to be widespread and important in the evolution of sex. Because in this model epidemics alternate with periods of high host resistance, leading to ceaseless advances and retreats for both host and pathogen, we use the term 'trench warfare' rather than 'arms race' to describe the evolution of this host–pathogen interaction.

Resistance-allele frequencies in local populations throughout the northern hemisphere are generally high (Fig. 4), as required for our model to accommodate the sequence data. A striking exception is the midwest United States, where resistance-allele frequencies are much lower than our model predicts. This indicates that the pathogen recognized by *Rpm1* may not be prevalent in the midwest.

We note that our model is deterministic, and in finite populations drift and founder effects can lead to the rapid loss of variation in local populations, whereas geographic variation can help to maintain polymorphism in the species as a whole[26]. Dynamical polymorphism is the hallmark of the trench-warfare hypothesis, but, considering the effects of drift, trench warfare might not always lead to the long-term maintenance of variation for disease resistance.

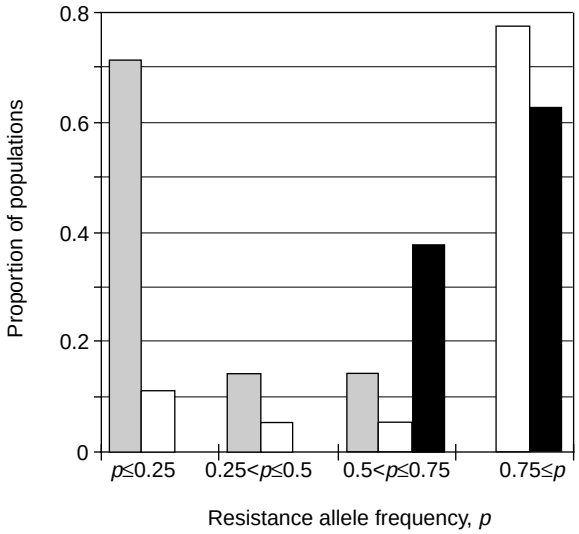

Figure 4 Resistance-allele frequency distributions. The proportion of populations with *Rpm1* resistance-allele frequencies in the indicated range for the United States midwest (stippled bars, 21 populations) and for the northern hemisphere excluding the US midwest (white bars, 19 populations) are compared with that predicted by our model for an *A. thaliana*–*Pseudomonas* interaction (black bars). The predicted distribution is the proportion of time during each cycle that the resistance allele spends in each frequency category, assuming that each population represents an independent random time point under the model. About ten individuals were sampled from each population.

Thus, the finding of a recently evolved disease resistance polymorphism in *Arabidopsis*, *Rps2* (ref. 27), is not inconsistent with the trench-warfare hypothesis. Population genetic studies of additional disease-resistance loci will be needed to evaluate the generality of this trench warfare model. Information on the ecological dynamics and demography of disease resistance provided by these studies should be valuable in applied contexts. □

Methods

Plant materials and phenotyping. Seeds of 26 accessions (Table 1) and *A. lyrata* were taken from the collections of J.B. and R.M., or received from the *Arabidopsis* stock centres. Accessions were phenotyped for *Rpm1* disease resistance by dipping plants in liquid cultures of *Pseudomonas syringae* DC3000 (control) or DC3000::AvrRpm1 (from J. Dangl), noting resistance response or disease symptoms after four days[8]. DNA from 447 individuals representing 40 populations of *A. thaliana* were assembled from the collections of J.B., R.M. and N. Miyashita. Seed stocks have been donated to the ABRC. Seeds were germinated in the greenhouse, and DNA was extracted according to standard protocols[28].

Genotyping. The *Rpm1* junction region sequence (J. Dangl and M. Grant, unpublished data) was extended to 2 kilobases (kb) 5′ and 1 kb 3′ of the junction, by inverse PCR, cloning and sequencing of accessions La-er and Nd-0. We used these sequences to design primers. A three-primer PCR (primers 1190^{+} TCGTGATTCCATTTGCTTGTA, $R1^{-}$ TCGGGTGTTGTTTTCGTCAT and $S1^{-}$ GTGGAGCAAAAAGAGATGTG, designed by G. Wichman) gives alternative products for resistance and susceptibility alleles. Before cloning and/or sequencing the resistance alleles, the junction region was amplified using 5′ primers ($R5J^{+}$ CCCCGAGAGGCTGCTGAGAAATGGC and $R5I^{-}$ CCATCATCAATAGGCGGTAATAATGCTGC) and 3′ primers ($R3I^{+}$ CGGTCAAGGGTTAAACACATTCCTGC and $R3J^{-}$ AACGGATCATCATTATTTCAAGTACATCACATCGC). Susceptibility alleles were amplified using $R5J^{+}$ and $R3J^{-}$. An *A. lyrata* allele, including the junction region and the intronless *Rpm1* coding sequence, was assembled by shotgun-cloning and sequencing a long-PCR product (primers $R5J^{+}$ and $R3J^{-}$). Cloning was into a modified pZero 2.1 vector (Strategene), and sequences were generated from PCR products of multiple colonies. The flanking sequences and the *A. lyrata* coding sequence have Genbank accession numbers AF122981–AF123027. Aligned flanking sequences are available from the author.

Population genetics analyses. We performed Tajima's D test[15], sliding window analyses and silent and replacement divergence[22] estimation using DNAsp[29]. Runs tests used the DNASlider program[16], with recombination parameters from 0 to 32 (10,000 replicates for conservative recombination values). Population structure in *A. thaliana* was studied under a two-subpopulation equilibrium migration model[30], conditional on the numbers of segregating sites, using simulation code from R. Hudson. We chose the migration parameter to maximize the probability of the homozygosity of derived mutations in several published datasets[17–20].

Balancing selection at a constant frequency was studied over a range of frequencies by simulation (10,000 replicates), assuming that samples of 14 resistance and 13 susceptibility alleles coalesce independently at rates proportional to their relative frequencies[13] without recombination, and that the sum of the number of intraclass polymorphisms for the two allelic classes equals the observed sum of 15. We calculated the mean number of polymorphisms and the probability of 12 or more polymorphisms within the resistance allelic class.

Ecological modelling. In the absence of field observations of interactions between *A. thaliana* and *Pseudomonas*, we based our model on the biology of each species. Because *rpm1* is a deletion, it cannot encode specificity for an alternative pathogen. We assume that *P. syringae* strains that interact with *Rpm1* are specific to *A. thaliana*. Given *A. thaliana*'s low heterozygosity[28], we assume a haploid host. We begin with an equation for host resistance allele frequency p_t in generation t,

$$p_t = \frac{p_{t-1}}{p_{t-1} + \theta(1 - p_{t-1})(1 - I)} \quad (1)$$

θ is the ratio of the fitnesses of uninfected susceptible and resistant individuals and I is the fraction of infected susceptible individuals. Infected susceptible individuals are assumed to have zero fitness, although a low nonzero fitness does not affect our results. Importantly, epiphytic populations of *Pseudomonas* on non-host plants contribute to subsequent epidemics[23]. Pathogen density z_t during host generation t is determined by

$$z_t = \lambda K(1 - p_{t-1})I + \gamma z_{t-1} \quad (2)$$

Here λ is epiphytic population growth between epidemics, K is host population density, and γ is long-term survival of pathogens. We use an SIR model[11] to give the proportion of susceptible individuals that are infected,

$$I = 1 - \exp(R_0 I(1 - p_t) + z_t/N_T) \quad (3)$$

Here R_O is the fitness of pathogens produced during the epidemic and N_T is the threshold population density.

Re-scaling z_t according to $\hat{z}_t = z_t/N_T$ shows that the dynamics depend only on θ, R_O and a parameter $\hat{R}_o = \lambda K/N_T$, the fitness of pathogens from the previous epidemic. Costs of resistance average 7%[22]; therefore, we set $\theta = 1/0.93 = 1.08$. We fit the model to the ratio of average pairwise distances within *Rpm1* resistance and susceptibility allelic classes $\pi_R/\pi_S = 5.71$, and to the sampled resistance-allele frequency 0.52. We calculated the expected ratio of average pairwise distances within allelic classes using a standard coalescence formula[10], into which we substituted harmonic means of resistance and susceptibility allele frequencies from model runs of 10,000 generations (discarding transients). The resulting parameter estimates are $R_O = 1.35$, $\hat{R}_o = 2.23$ and $\gamma = 0.2$; the expected ratio of average pairwise distances within allelic classes is 5.7, and the frequency of resistance lies within ± 0.05 of the estimated frequency 13% of the time.

Received 25 March; accepted 7 June 1999.

1. Dawkins, R. & Krebs, J. R. Arms race between and within species. *Proc. R. Soc. Lond. B* **205,** 489–511 (1979).
2. Kunkel, B. A useful weed put to work: genetic analysis of disease resistance loci in *Arabidopsis thaliana*. *Trends Genet.* **12,** 63–69 (1996).
3. Grant, M. R. *et al.* Structure of the *Arabidopsis RPM1* gene enabling dual specificity disease resistance. *Science* **269,** 843–846 (1995).
4. Jayakar, S. D. A mathematical model for interaction of gene frequencies in a parasite and its host. *Theor. Popul. Biol.* **1,** 140–164 (1970).
5. Hamilton, W. D. in *Population Biology of Infectious Diseases* (eds Anderson, R. M. & May, R. M.) 269–296 (Springer, Berlin, 1982).
6. Grant, M. R. *et al.* Independent deletions of a pathogen-resistance gene in *Brassica* and *Arabidopsis*. *Proc. Natl Acad. Sci. USA* **95,** 15843–15848 (1998).
7. O'Kane, S. L. & Al-Shehbaz, I. A synopsis of *Arabidopsis* (Brassicaceae). *Novon* **7,** 323–327 (1997).

8. Whalen, M. C., Innes, R. W., Bent, A. F. & Staskawicz, B. J. Identification of *Pseudomonas syringae* pathogens of *Arabidopsis* and a bacterial locus determining avirulence on both *Arabidopsis* and soybean. *Plant Cell* **3,** 49–59 (1991).
9. May, R. M. in *Ecology and Genetics of Host-Parasite Interactions* (eds Rollinson, D. & Anderson, R. M.) 243–262 (Academic, New York, 1985).
10. Maynard Smith, J. & Haigh, J. The hitchhiking effect of a favourable gene. *Genet. Res.* **23,** 23–25 (1974).
11. May, R. M. & Anderson, R. M. Epidemiology and genetics in the coevolution of parasites and hosts. *Proc. R. Soc. Lond. B* **219,** 281–313 (1983).
12. Hamilton, W. D., Axelrod, R. & Tanese, R. Sexual reproduction as an adaptation to resist parasites (a review). *Proc. Natl Acad. Sci. USA* **87,** 3566–3573 (1990).
13. Hudson, R. R. & Kaplan, N. L. The coalescent process in models with selection and recombination. *Genetics* **120,** 831–840 (1988).
14. Kimura, M. *The Neutral Theory of Molecular Evolution* (Cambridge Univ. Press, Cambridge, 1983).
15. Tajima, F. Statistical method for testing the neutral mutation hypothesis by DNA polymorphism. *Genetics* **123,** 585–595 (1989).
16. McDonald, J. H. Improved tests for heterogenity across a region of DNA sequence in the ratio of polymorphism to divergence. *Mol. Biol. Evol.* **15,** 377–384 (1998).
17. Innan, H., Tajima, F., Terauchi, R. & Miyashita, N. T. Intragenic recombination in the *Adh* locus of the wild plant *Arabidopsis thaliana*. *Genetics* **143,** 1761–1770 (1996).
18. Kawabe, A., Innan, H., Terauchi, R. & Miyashita, N. T. Nucleotide polymorphism in the acidic chitinase locus (ChiA) region of the wild plant *Arabidopsis thaliana*. *Mol. Biol. Evol.* **14,** 1303–1315 (1997).
19. Purugganan, M. D. & Suddith, J. I. Molecular population genetics of the *Arabidopsis* CAULIFLOWER regulatory gene: nonneutral evolution and naturally occurring variation in floral homeotic function. *Proc. Natl Acad. Sci. USA* **95,** 8130–8134 (1998).
20. Purugganan, M. D. & Suddith, J. I. Molecular population genetics of floral homeotic loci: departures from the equilibrium-neutral model at the *APETALA3* and *PISTILLATA* genes of *Arabidopsis thaliana*. *Genetics* **151,** 839–848 (1999).
21. Wolfe, K. H., Sharp, P. M. & Li, W.-H. Rates of synonymous substitution in plant nuclear genes. *J. Mol. Evol.* **29,** 208–211 (1989).
22. Nei, M. & Gojobori, T. Simple methods for estimating the numbers of synonymous and non-synonymous nucleotide substitutions. *Mol. Biol. Evol.* **3,** 418–426 (1986).
23. Redei, G. P. *Arabidopsis* as a genetic tool. *Annu. Rev. Genet.* **9,** 111–127 (1986).
24. Bergelson, J. & Purrington, C. Surveying patterns in the cost of resistance in plants. *Am. Nat.* **148,** 536–558 (1996).
25. Hirano, S. S. & Upper, C. D. Population biology and epidemiology of *Pseudomonas syringae*. *Annu. Rev. Phytopath.* **28,** 155–177 (1990).
26. Judson, O. Preserving genes: a model of the maintenance of genetic variation in a metapopulation under frequency-dependent selection. *Genet. Res. Camb.* **65,** 175–191 (1995).
27. Caicedo, A. L., Schaal, B. A. & Kunkel, B. N. Diversity and molecular evolution of the *RPS2* resistance gene in *Arabidopsis thaliana*. *Proc. Natl Acad. Sci. USA* **96,** 302–306 (1999).
28. Bergelson, J., Stahl, E., Dudek, S. & Kreitman, M. Genetic variation within and among populations of *Arabidopsis thaliana*. *Genetics* **148,** 1311–1323 (1998).
29. Rozas, J. & Rozas, R. DnaSP version 2.0: A novel software package for extensive molecular population genetics analysis. *Comput. Appl. Biosci.* **13,** 307–311 (1997).
30. Hudson, R. R. in *Oxford Surveys in Evolutionary Biology* Vol. 7 (eds Futuyama, D. & Antonovics, J.) 1–44 (Oxford Univ. Press, Oxford, 1990).

Acknowledgements. M. Grant and J. McDowell provided unpublished sequences, and R. Hudson provided computer code. The Nottingham and Ohio State University *Arabidopsis* stock centres provided seeds. We thank R. Hudson, H. Innan, A. Kawabe, C. Langley, Y. Satta and N. Takahata for helpful discussions, and J. Dangl, P. Kareiva, S. Levin and J. McDowell for commenting on earlier versions of the manuscript. G.D. was supported by a Dropkin fellowship and R.M. was supported by an NSF/Sloan Fellowship in Molecular Evolution. This work was supported by an NSF Presidential Award and Packard Fellowship to J.B., an NIH grant to M.K., an NIH grant to J.B. and M.K. and a University of Chicago Hinds Fund grant to E.A.S.

Correspondence and requests for materials should be addressed to J.B. (e-mail: jbergels@midway.uchicago.edu).

Time-dependent reorganization of brain circuitry underlying long-term memory storage

Bruno Bontempi, Catherine Laurent-Demir, Claude Destrade & Robert Jaffard

Laboratoire de Neurosciences Cognitives, CNRS UMR 5807, Université Bordeaux I, Avenue des Facultés, 33405 Talence, France

Retrograde amnesia observed following hippocampal lesions in humans and animals is typically temporally graded[1,2], with recent memory being impaired while remote memories remain intact, indicating that the hippocampal formation has a time-limited role in memory storage[3,4]. However, this claim remains controversial because studies involving hippocampal lesions tell us nothing about the contribution of the hippocampus to memory storage if this region was present at the time of memory retrieval[5,6]. We therefore used non-invasive functional brain imaging using (^{14}C)2-deoxyglucose uptake to examine how the brain circuitry underlying long-term memory storage is reorganized over time in an intact brain. Regional metabolic activity in the brain was mapped in mice tested at different times for retention of a spatial discrimination task. Here we report that increasing the retention interval from 5 days to 25 days resulted in both decreased hippocampal metabolic activity during retention testing and a loss of correlation between hippocampal metabolic activity and memory performance. Concomitantly, a recruitment of certain cortical areas was observed. These results indicate that there is a time-dependent reorganization of the neuronal circuitry underlying long-term memory storage, in which a transitory interaction between the hippocampal formation and the neocortex would mediate the establishment of long-lived cortical memory representations.

The phenomenon of temporally graded retrograde amnesia constitutes a major argument for a memory consolidation process being required for stable memory formation[7]. Although it is generally accepted that this process involves a stabilization of synaptic modifications after a learning experience, regardless of which brain system is involved, it is not yet clear how different systems in an intact brain reorganize over an extended period of time to support long-term memory storage[8,9]. We therefore mapped (^{14}C)2-deoxyglucose uptake[10] in selected brain regions of the mouse to measure regional metabolic activity associated with retrieval testing of a recently versus remotely acquired spatial discrimination task. Our objective was to understand the roles of the hippocampal formation and the cortical areas during memory consolidation.

An intrajugular catheter[11] was attached to male BALB/c mice that were trained over nine consecutive daily sessions in an eight-arm radial maze to discriminate the three arms that were constantly baited with food from the five arms that were never baited. After a retention interval of either 5 days (5-day retention group; $n = 9$) or 25 days (25-day retention group; $n = 8$), chosen according to data obtained from previous lesion experiments[12], animals were tested once under the same conditions as the initial acquisition. To examine whether changes in functional metabolic activity of the hippocampal formation at the 25-day retention interval are specifically related to the previously learned information, two additional groups of mice were tested under different conditions. Animals were placed either in the same maze as the initial acquisition but with a different location of food (same context/different arms group; $n = 7$) or in a different maze located in a different room (different context/different arms group; $n = 8$) with respect to initial acquisition. Finally, two control groups included mice that were submitted only to the nine initial training sessions (acquisition group; $n = 7$) and mice that were maintained in their home cages ('quiet' control group; $n = 8$) during the experimental period. Levels of regional

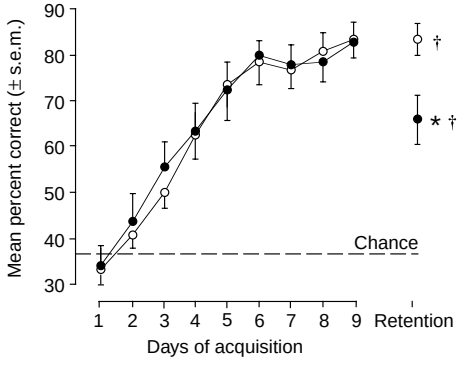

Figure 1 Curves showing the progression of spatial discrimination performance over the nine daily sessions of initial acquisition and the retention performance of the 5-day (open circles) and 25-day (filled circles) retention groups. *$P < 0.05$ as compared to the 5-day retention group; †$P < 0.005$ as compared to chance level.